AGU PUBLICATIONS

Geophysical Research Letters

RESEARCH LETTER
10.1002/2017GL073531

Key Points:
- The areas affected by heat waves have increased over China during the recent five decades
- Anthropogenic influences will cause a greater than tenfold increase in the likelihood of the strongest heat wave on record across more than half China
- The extremes in heat distribution are more sensitive to precipitation deficits over the eastern Chinas

Supporting Information:
- Supporting Information S1

Correspondence to:
C. Miao,
miaocy@vip.sina.com

Citation:
Sun, Q., C. Miao, A. AghaKouchak, and Q. Duan (2017), Unraveling anthropogenic influence on the changing risk of heat waves in China, *Geophys. Res. Lett.*, *44*, 5078–5085, doi:10.1002/2017GL073531.

Received 20 MAR 2017
Accepted 28 APR 2017
Accepted article online 3 MAY 2017
Published online 21 MAY 2017

Unraveling anthropogenic influence on the changing risk of heat waves in China

Qiaohong Sun[1,2], Chiyuan Miao[1], Amir AghaKouchak[2], and Qingyun Duan[1]

[1]State Key Laboratory of Earth Surface Processes and Resource Ecology, Faculty of Geographical Science, Beijing Normal University, Beijing, China, [2]Center for Hydrometeorology and Remote Sensing, Department of Civil and Environmental Engineering, University of California, Irvine, California, USA

Abstract Heat waves trigger substantial social and environmental impacts and even cause massive civilian casualties in extreme cases. Observations show the areas affected by heat waves have increased over China, with the most extreme heat wave occurring during the past five decades. Here we show that both trends can be attributed to anthropogenic influences. We report that under the moderate Representative Concentration Pathways 4.5 scenario, anthropogenic influences will increase the risk of occurrence of the observed maximum Heat Wave Magnitude Index in the late 21st century and will cause a more than tenfold increase in the likelihood of the strongest events on record recurring across more than half China. More than 50% of land area in China is projected to be affected by intense heat waves. Our results show that over eastern China, the extremes in heat distribution are more sensitive to precipitation deficits, indicating stronger heat wave amplification trends to occur under drier conditions. The likelihood of concurrent droughts and heat waves is expected to increase in large parts of China in the late 21st century.

1. Introduction

A heat wave is generally defined as a prolonged period of excessively hot weather. Recently, many studies have investigated the human contributions to extraordinary and record-breaking heat waves in different regions of the globe. At the global scale, warm spells and heat wave frequency, intensity, and duration have increased [*Perkins et al.*, 2012]. At the regional scale, it is very likely that human influence mainly contributed to the 2003 European heat wave [*Stott et al.*, 2004], and the 2010 severe heat wave in western Russia [*Hauser et al.*, 2016; *Otto et al.*, 2012; *Rahmstorf and Coumou*, 2011]. A crucial contributor to the formation of exceptionally high temperatures is land-atmosphere feedback, that is, soil moisture-temperature feedback [*Hauser et al.*, 2016; *Sun et al.*, 2016]. Observational data have provided evidence for a strong relationship between precipitation deficits and extreme temperatures in many regions, especially in Europe [*Mueller and Seneviratne*, 2013; *Quesada et al.*, 2012]. Soil moisture-temperature feedback was deemed important for the evolution of the 2003 European heat wave [*Fischer et al.*, 2007], the 2010 severe heat wave in western Russia [*Hauser et al.*, 2016], and the exceptional 2011 heat wave in Texas [*Mueller and Seneviratne*, 2013]. A lack of soil moisture may reduce latent cooling, amplifying surface temperature anomalies and increasing the risk of a severe heat wave.

In the context of global warming, positive trends in heat wave indices have been reported since 1990 over the whole of China [*You et al.*, 2016]. To enable climate adaptation and prediction of meteorological disasters, there has been an increase in efforts to attribute heat waves and predict their future likelihood. For example, models participating in the Coupled Model Intercomparison Project Phase 5 (CMIP5) showed that anthropogenic influences caused a more than sixtyfold increase in the likelihood of such events and that the evolution and characteristics of heat waves are correlated with deficits in precipitation [*Sun et al.*, 2014]. The combined effects of anthropogenic and natural forcings could explain the hot spring days in 2014, with human influences a dominant factor [*Song et al.*, 2015]. However, most previous studies focused on a specific event or on regional-averaged temperature. The characteristics of heat waves and their potential drivers are likely to vary from region to region within China because of its complex topography and diverse climate. Furthermore, potential heat-induced damage also varies from region to region because of uneven population distribution and agroecosystem diversity. A more detailed analysis of the occurrence of heat waves in China is therefore necessary. Better understanding of the evolution of heat events in China and their driving factors will help improve prediction and assessment of the impact of heat waves at regional and local scales. Many previous studies focused only on analysis of observed events; however, an understanding the

changing risk of heat waves in China for different periods in the future is essential for adjusting policies concerning adaptation to climate change.

In this study, therefore, we aim to investigate the maximum Heat Wave Magnitude Index (HWMI) value in 0.5° × 0.5° resolution grid boxes across China during the period 1961–2015, examine the potential factors affecting the occurrence of heat waves in China, and project the future spatial variability of heat wave risk in a warming climate. We examine the changes of heat wave and unravel the anthropogenic influence on the changing risk of heat waves in China based on high-intensity observations and global climate model (GCM) simulations involved in phase 5 of the Coupled Model Intercomparison Project (CMIP5).

2. Data and Methods

2.1. Models and Observations Used

Daily maximum temperatures from 2481 stations across China were collected from the SURF_CLI_CHN_MUL_DAY_V3.0 data set which was downloaded from the China Meteorological Data Sharing Service System (http://cdc.nmic.cn/home.do). The data were subject to strict quality controls and homogenized according to the methods described by *Xu et al.* [2013]. To maintain data consistency, we used data only from the 1681 stations that had fewer than 0.05% missing values. Missing values were replaced by adjacent values. The data were interpolated to 0.5° × 0.5° using the inverse distance weighting method. Gridded daily precipitation data developed by the National Meteorological Information Center of the China Meteorological Administration were used to evaluate dry/wet conditions and were constructed from over 2400 station observations across China at a resolution of 0.5° × 0.5°. The full data set was subject to strict quality controls according to the methods described by *Shen et al.* [2010]. We focused on the historical period 1961–2015.

Sixteen runs from seven GCM simulations involved in CMIP5 [*Taylor et al*., 2012] were used to assess the contribution of human influences to the observed heat waves (Table S1 in the supporting information, available at http://pcmdi9.llnl.gov/esgf-web-fe/). The simulations were first driven by natural forcing only and then by all forcings. The natural-forcing simulations include the natural variability (volcanic and solar activities), whereas the all-forcing simulations include both anthropogenic (well-mixed greenhouse gases, aerosols, ozone, and land use change) and natural forcing (volcanic and solar). Most models simulate natural and greenhouse gas responses only up to 2005, but our analysis period was 1961–2015. We thus used seven models that had historical and natural simulations extending through 2012. To enable comparison with observations, we used heat wave projections from the Representative Concentration Pathways 4.5 (RCP4.5) scenario to extend the time series of all-forcing simulations through 2015. Previous studies have shown that greenhouse gas forcing under the RCP4.5 scenario results in projections most consistent with current values in China [*Sun et al*., 2014; *Yang et al*., 2016]. Model projections under the RCP4.5 scenario were also used in this study for the period 2016–2099. To investigate trends in the future risk of heat waves, we used a 55 year moving window in the period 2016–2099, producing a total of thirty 55 year time periods (2016–2060, 2017–2061, 2018–2062, …, 2045–2099). We estimated heat wave risk index during each 55 year time period and then calculated the rate of change of the risk index at each grid location.

2.2. Defining Heat Wave Events

The Heat Wave Magnitude Index (HWMI) was developed by *Russo et al.* [2014] to quantify heat wave magnitude by taking the duration and intensity of heat waves into consideration. *Russo et al*. [2014] provide the details of HWMI Calculation, which is also available in "extRemes" R-package (open-source). The HWMI is defined as the maximum heat wave magnitude for a given year. HWMI values were calculated from the daily maximum temperatures, as follows. First, we defined a heat wave as a sequence of three or more days in which the daily maximum temperature was higher than the 90th percentile of daily maximum temperature, as calculated from a 31 day running window surrounding the day during the baseline period (1961–1990). Then, the maximum magnitude of the heat waves within a year (the HWMI) was determined. We divided the heat waves into different levels on the basis of the HWMI values: normal ($1 < \text{HWMI} < 2$), moderate ($2 \leq \text{HWMI} < 3$), intense ($\text{HWMI} \geq 3$).

2.3. Attribution Method

We used the fraction of attributable risk (FAR) and a related "risk index" [*Stott et al*., 2004] to assess the causes of extreme heat. First, a generalized extreme value (GEV) distribution was used to fit the HWMI time series.

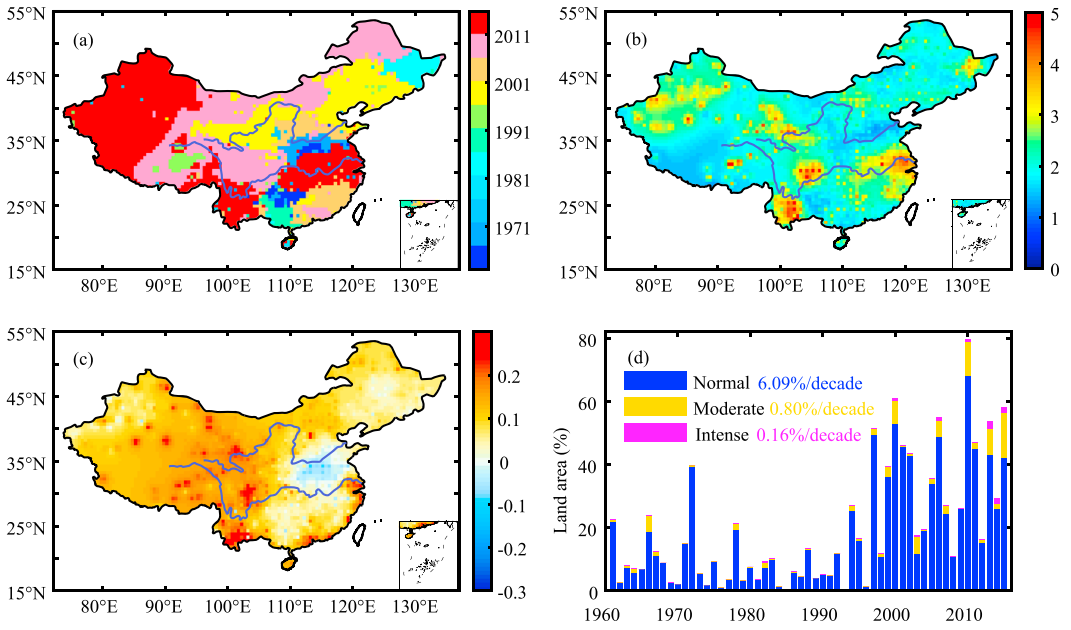

Figure 1. Spatial distribution of observed Heat Wave Magnitude Index (HWMI) values during the period 1961–2015. (a) Year in which the maximum heat wave occurred. (b) Maximum HWMI values. (c) Decadal changes in HWMI values (absolute change in the HWMI value per decade). (d) Percentage of land area affected by different heat wave levels over time (blue: $1 < \text{HWMI} < 2$; yellow: $2 \le \text{HWMI} < 3$; magenta: $\text{HWMI} \ge 3$). The colored text indicates the corresponding changes in HWMI for the affected areas.

The Kolmogorov-Smirnov (K-S) goodness-of-fit test was used to verify the fit of the distribution. To ascertain the contribution of anthropogenic climate change to risk of heat waves, we compared the probability that the observed maximum heat wave would occur in the all-forcings simulation with the probability that it would occur in the natural-forcing simulation. The equations are

$$\text{FAR} = 1 - P_{\text{nat}}/P_{\text{all}} \tag{1}$$

$$\text{Risk index} = P_{\text{all}}/P_{\text{nat}} \tag{2}$$

where P_{all} and P_{nat} are the probability that the observed events occur in the all-forcings and natural-forcing simulations, respectively.

We used the standardized precipitation index (SPI) [*McKee et al.*, 1993] as a measure of dry/wet conditions. The SPI quantifies observed precipitation as departures from a model of the raw precipitation data and was estimated for the period 1961–2015 from monthly precipitation data sets. Quantile regression (see supporting information) estimates conditional quantile values at each part of a distribution from a regression as a function of a conditional parameter [*Koenker and Hallock*, 2001] and was applied to estimate the relationship between heat waves and the preceding (or concurrent) SPI.

3. Results

3.1. Detection and Attribution of Heat Waves

Over large parts of China, the strongest heat wave occurred in recent decades (Figure 1a). The related heat wave magnitudes reached intense levels, with HWMI values greater than 3 in the lower reaches of the Yangtze River basin, southeastern China, the upper reaches of the Yellow River basin, and southwestern China (Figure 1b). The HWMI values trend upward in almost all grid locations (84.80%) apart from China's north plain, indicating an increase in the severity of heat waves during this time period. The slightly decreasing trends in China's north plain may be related to the increased precipitation associated with the weakened westerly over East Asia [*Zhu et al.*, 2011], leading to less extreme heat days [*Lu and Chen*, 2016; *You et al.*, 2016]. The upward trend is more remarkable in western China than eastern China (Figure 1c). With climate

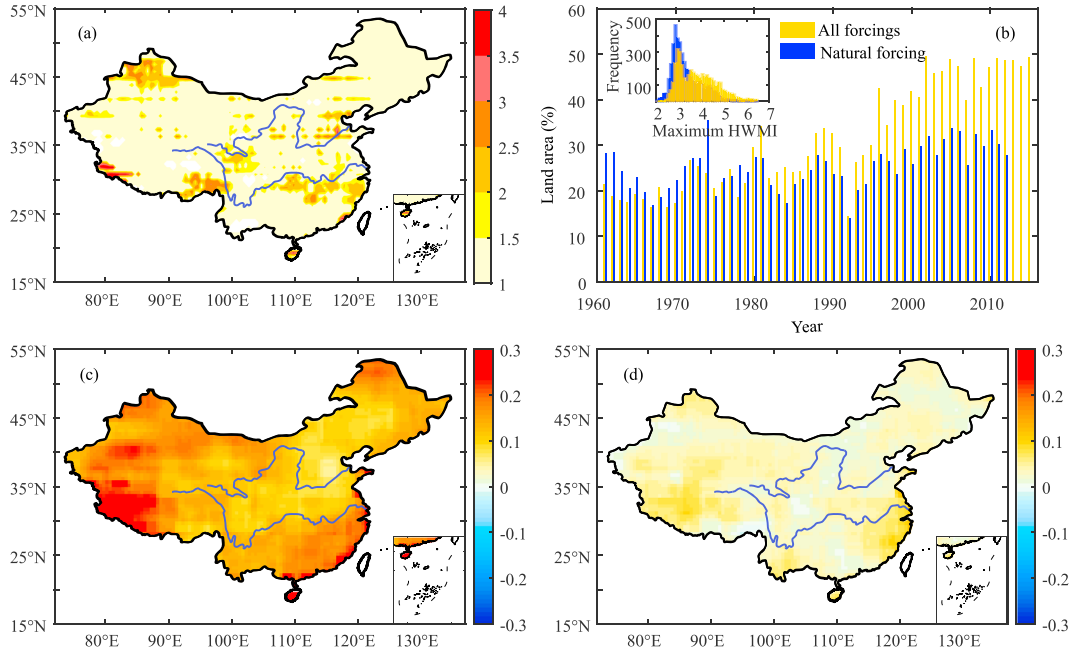

Figure 2. Simulated Heat Wave Magnitude Index (HWMI) values with natural forcing and all forcings (including natural and anthropogenic). (a) Risk index for the observed maximum heat wave at each grid location during the period 1961–2015. (b) Percentage of land area affected by heat waves with HWMI > 1. Inset: histograms of the maximum HWMI value at each grid location for the period 1961–2012 under either the natural-forcing or the all-forcings simulation. (c) Decadal changes in HWMI values for the period 1961–2012 in the all-forcings simulation (absolute change in the HWMI value per decade). (d) Decadal changes in HWMI values for the period 1961–2012 in the natural-forcing simulation (absolute change in the HWMI value per decade).

warming, a greater area of land is suffering more frequent and more severe heat waves. The land area affected by different heat wave levels has enlarged in recent years (Figure 1d).

We examined the factors contributing to the unusual heat waves occurring over China. For each grid location, we compared the likelihood of the observed maximum HWMI value occurring in different CMIP5 experiments. Over large parts of China, the risk index (equation (2) is greater than 1 (Figure 2a), indicating an increased likelihood of strong heat waves when anthropogenic influences are included. For grids located in the Yangtze River basin, the lower and upper reaches of the Yellow River basin, southwestern China, and northwestern China, anthropogenic factors cause a more than twofold increase in the probability of occurrence of a heat wave as intense as the maximum observed HWMI. Attribution studies on the 2013 summer heat in eastern China and the July 2015 record-breaking heat in northwestern China have demonstrated that anthropogenic influences increased the likelihood of these extreme heat events [*Miao et al*., 2016; *Sun et al*., 2014]. As anthropogenic climate change has increased, more and more regions in China have experienced heat waves, especially from the late twentieth century onward (Figure 2b). More than half of mainland China is now expected to suffer from heat waves when all forcings are included in the simulations. Furthermore, the distribution of simulated maximum HWMI values is shifted to the right in the all-forcings experiment compared with the natural-forcing experiment (Figure 2b, inset), indicating an increase in the frequency, duration, and intensity of extreme heat waves in China when human factors are included. The contrasting trends in HWMI in the all-forcings and natural-forcing simulations provide more evidence of the likelihood that the HWMI values are affected by human factors in China (Figures 2c and 2d). The pattern of simulated HWMI trends is similar to the pattern of observed HWMI trends, with upward trends in most regions (Figures 1c and 2c). However, there are some differences between the observations and the all-forcings simulation in northern China, with small downward trends in the observations but upward trends in the model simulations.

The relationship between heat waves and either the SPI from the preceding month or the concurrent SPI are shown in Figure 3. Large parts of eastern, northern, and southwestern China have a negative correlation

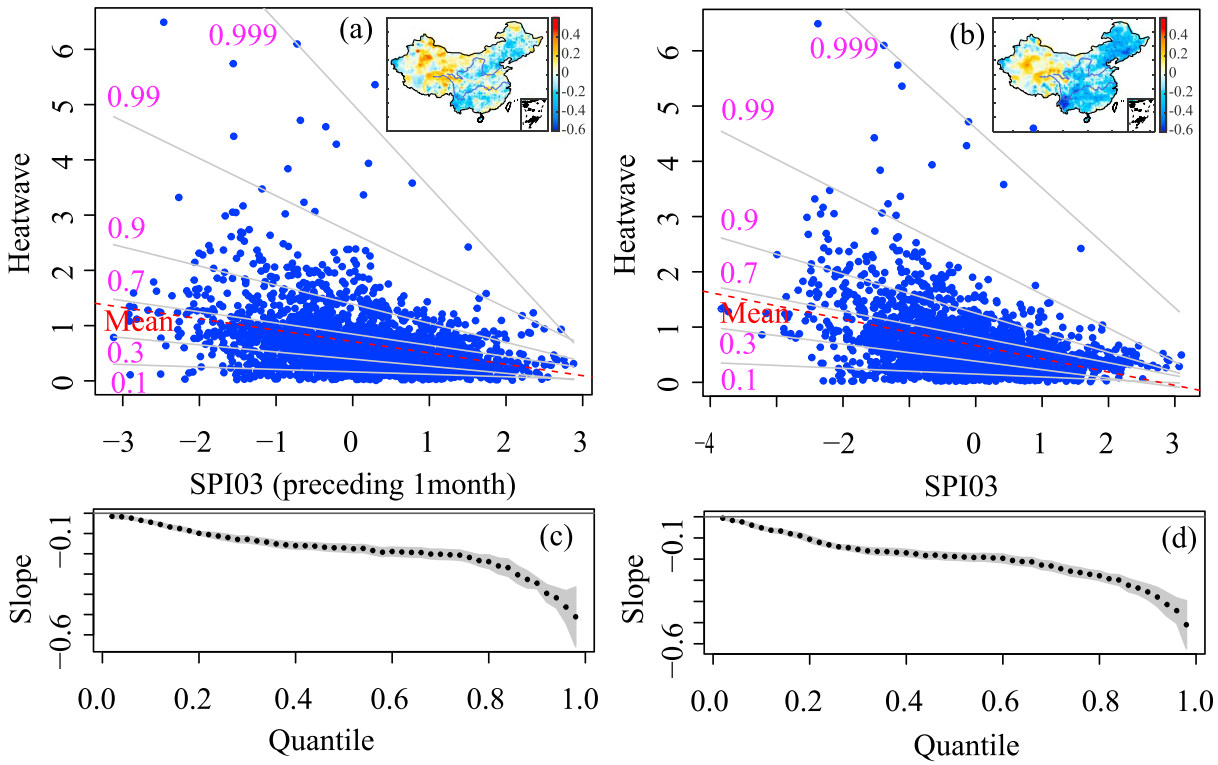

Figure 3. Understanding the relationship between heat waves and precipitation deficit. Quantile regression analysis for heat waves and the standardized precipitation index (SPI). Scatterplots of the maximum HWDI values during the period 1961–2015 for each grid location versus (a) the SPI from the preceding 1 months and (b) the concurrent SPI. Insets: spatial distribution of the correlation coefficients for HWMI and the corresponding SPI values. Regression slopes for the 0.01–0.99 quantiles of the maximum HWDI values in relation to (c) the SPI from the preceding 1 months and (d) concurrent SPI. Black dots indicate the regression slope for the different quantiles and shading indicates the associated uncertainty range.

between the maximum HWMI value and the preceding dry/wet conditions (SPI), indicating that heat waves are likely to occur after dry conditions. Data from grid locations with a statistically significant ($p < 0.01$) correlation between the maximum HWMI value and SPI were used to estimate the slope of the relationship at different quantiles (quantile regression). The slope increases with the quantiles (Figures 3a and 3c), indicating that the intensity of a heat wave is sensitive to the preceding dry/wet conditions: Stronger heat waves tend to occur after drier conditions. However, there is a positive relationship between HWMI and SPI in northwest China. This arid and semiarid region has become wetter in recent decades probably because of the strengthening of the North America Subtropical High and the West Pacific Subtropical High after the mid-1980s [*Li et al.*, 2016].

Droughts and heat waves can occur simultaneously, intensifying the severity of and damage from each [*AghaKouchak et al.*, 2014; *Mazdiyasni and AghaKouchak*, 2015; *Yang et al.*, 2017]. Eastern China is more vulnerable to the influence of compound heat waves and droughts, with strong negative correlations between the concurrent SPI and HWMI (Figure 3b). The slope of the regression between concurrent HWMI and SPI is in the same direction for all quantiles and the slope increases in the higher quantiles (Figure 3d). Drought conditions are conducive to the occurrence of heat extremes and heat waves reinforce the severity of droughts, thereby increasing the probability of simultaneous occurrence of extreme heat waves and droughts.

3.2. Changing Heat Wave Risk Under Future Climate Conditions

Under the RCP4.5 scenario, the land area affected by heat waves is projected to increase during the period 2016–2099 (Figure 4a). The total area affected by normal and moderate heat waves is projected to decrease, but the area affected by intense heat waves is projected to increase to approximately 50% of total land area in China by the late 21st century. The duration and severity of the most intense heat waves are also projected to

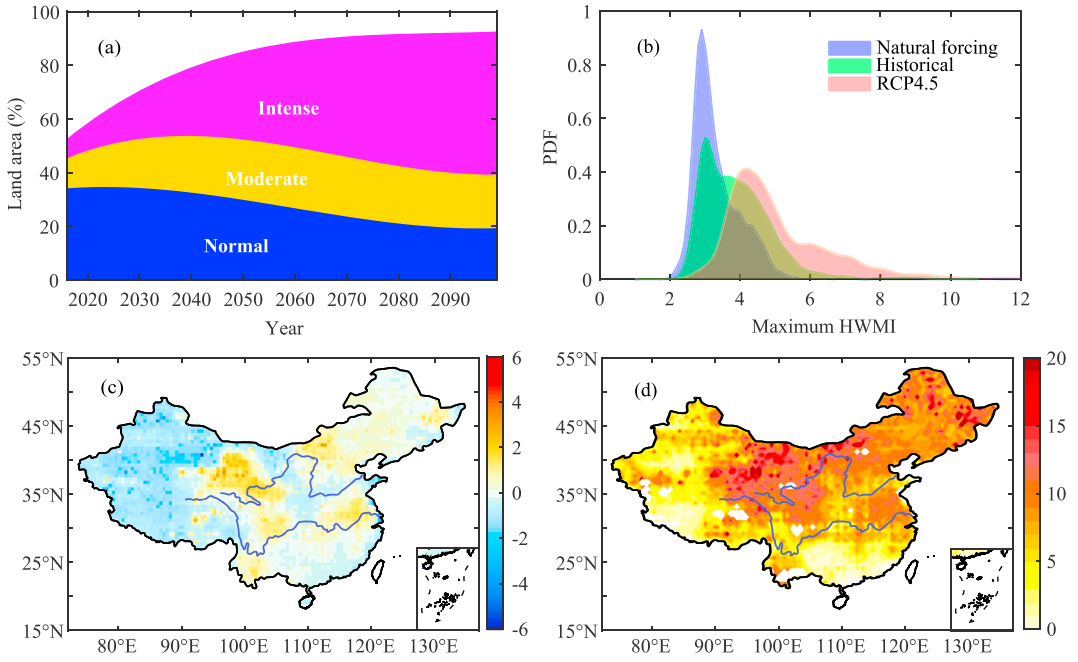

Figure 4. Projected Heat Wave Magnitude Index (HWMI) values under the RCP4.5 scenario. (a) Percentage of land area affected by different heat wave levels (blue: $1 < \text{HWMI} < 2$; yellow: $2 \leq \text{HWMI} < 3$; magenta: $\text{HWMI} \geq 3$) under the RCP4.5 scenario during the period 2016–2099. (b) Probability density functions (PDFs) for the occurrence of the maximum HWMI for all grid locations in the natural forcing (1961–2012), historical (1961–2015), and RCP4.5 (2045–2099) experiments. (c) Absolute change in the risk index value per decade, calculated for each grid location from 55 year moving windows over the period 2016–2099 under the RCP4.5 scenario. (d) Differences in the risk index for the observed maximum HWMI between the 2045–2099 period, under RCP4.5, and the 1961–2015 period.

increase; the distribution of the maximum HWMI values is shifted to the right under the RCP4.5 scenario, indicating an increased likelihood of extreme ($\text{HWMI} > 4$) and even very extreme ($\text{HWMI} > 8$) heat waves (Figure 4b). We estimated how the risk of heat waves changes in the future, under the assumption that future natural variability is stationary. We used thirty 55 year moving windows over the period 2016–2099 to obtain 30 risk factors under the RCP4.5 scenario for each grid location. For each grid location and each 55 year time period, we calculated the risk that there would be a future heat wave as strong as the most intense heat wave observed during the 1961–2015 period. Figure 4c shows that the risk progressively increases with anthropogenic warming in most northern China regions, the lower reaches of Yangtze River basin, and in various grid locations scattered in southwestern China, even though radiative forcing in the scenario starts to level off after the 2060s. In these regions, anthropogenic influences are projected to cause a more than tenfold increase in the likelihood of the current on-record maximum heat wave recurring during the 2045–2099 period under the RCP4.5 emissions scenario (Figure 4d). Overall, the risk of future heat waves is much stronger for northern China than for southern China, which reflects the different future warming rates in the north and the south.

The interaction between the occurrence of heat waves and droughts is important both for prediction and for disaster evaluation. Understanding the heat wave risk requires knowledge of this interaction. We project an increase in the frequency with which heat waves rapidly follow droughts in eastern China (Figure 5a). Understanding the relationship between heat waves and droughts is conducive to the prevention of heat waves. The risk of compound warm and dry events is higher in eastern China than in northwestern China. The likelihood of concurrent extreme events is expected to increase in large parts of China, with a higher frequency of concurrent droughts and heat waves in the 2045–2099 period compared with the 2016–2070 period.

4. Discussion and Conclusions

Here we present a heat wave detection and attribution analysis for the period 1961–2015 in China. Using high-density observations, we found that the areas affected by heat waves have increased in recent

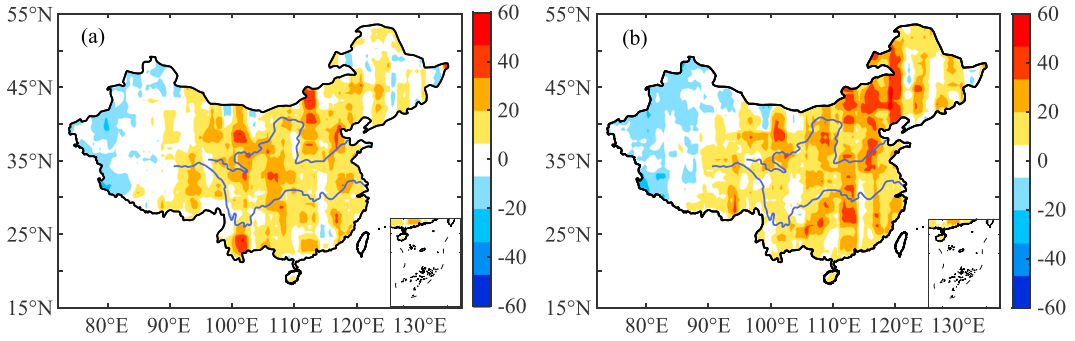

Figure 5. Percent change in the frequency of concurrent heat waves (HWMI $>$ 1) and droughts (SPI $<$ -1) during 2045–2099 relative to 2016–2070 under the RCP4.5 scenario. (a) Percent change in heat waves occurring after a preceding drought. (b) Percent change in heat waves occurring concurrently with drought.

decades and that for large regions of the country, the maximum heat wave occurred during the most recent decades. Southwestern China, the lower and middle reaches of the Yangtze River basin, and northwestern China have all suffered from record-breaking heat since 2011, which may in part be due to climate warming. Model simulations based on different forcings show that the patterns of change in the observations were most similar to those in the model when anthropogenic influences were included. Under the moderate RCP4.5 scenario, anthropogenic influences increase the risk of occurrence of the observed maximum HWMI in the late 21st century. Across more than half of China, anthropogenic forcings cause a more than tenfold increase in the likelihood of the strongest events on record recurring. In the future, heat waves that are unusual under the present climate conditions will occur on a regular basis and heat waves of greater severity and longer duration are projected to occur more frequently and in more regions. With both the frequency and severity of heat waves on an upward trajectory, the damaging effects of extreme heat waves in China will become more apparent over the next few decades. For instance, in eastern China, the risks associated with increased exposure to extreme heat are compounded by the large human population in that region [*Jones et al*., 2015]. Furthermore, the elderly and the ill are more susceptible to the effects of extreme heat [*Schär*, 2015]. With an increasing and aging population, the threat to human health from heat waves in the current century may be more severe than previously thought; thus, efforts to mitigate the effects of heat waves are essential for the inhabitants of China.

The dry/wet conditions preceding heat waves are a factor in heat wave evolution and severity in many areas of the world [*Meng and Shen*, 2014; *Miralles et al*., 2014; *Quesada et al*., 2012]. We identified a negative relationship between heat waves and the preceding and concurrent dry/wet conditions in large parts of eastern China, with SPI having an asymmetrical impact on heat. The negative slopes in the quantile regression gradually increased with the quantile, indicating that the high tail of the heat distribution is more sensitive to precipitation deficits: Stronger heat wave amplification tends to follow drier conditions [*Quesada et al*., 2012]. The index of precipitation deficits is generally regarded as an indication of soil moisture deficits [*Mueller and Seneviratne*, 2013]. Previous studies have suggested that the effects of soil moisture on near-surface climate are related to changes in temperature: Whenever soil moisture limits the total energy for latent heat flux, more energy is available for sensible heating, inducing an increase in near-surface air temperatures that can lead to extreme temperatures and heat waves [*Seneviratne et al*., 2010]. The associated soil moisture memory is important initial information and should enable more accurate predictions of extreme temperatures. However, the soil moisture-temperature interactions are complex and vary on spatial and temporal scales, so increased monitoring and model simulations are required to map out their relationship in different climate zones. In the future, droughts and heat waves are projected to occur simultaneously more often and reinforce each other over eastern China. The compound effects from simultaneous heat waves and droughts induce enormous losses in ecological and social systems. Extreme high temperatures and low precipitation reduce water availability and pose a great threat to agriculture and human health as well as an increased risk of wildfires. In a warming climate, the probability of concurrent events is projected to increase over large parts of China except in the northwest regions. A multivariate risk assessment is therefore required to develop suitable adaptation measures.

The occurrence of record-breaking heat can be mainly attributed to anthropogenic influences, heat wave severity is affected by land-atmosphere feedback, and the risk of longer, stronger heat waves that occur concurrently with other climate extremes is increased under the RCP4.5 future emissions scenario. However, heat wave evolution and variability is also related to natural variability including changes in climatic oscillations, volcanic activities, and sea temperatures. These potential drivers can also change and evolve over time and alter the risk of future heatwaves. Taking climate indices as covariates or using sensitivity experiments based on model simulations can shed light on the effects of changes in natural variability and the corresponding impacts on occurrence and severity of future heatwaves. In this study, the severity of heat wave shows some grid dependence, which may be related to the local factors, such as the urbanization, topography, and land use change. Occurrence of heat waves and their future changes under multiple compounding drivers deserves more research in the future.

Acknowledgments
This research was supported by the National Natural Science Foundation of China (41622101 and 91547118), the National Key Research and Development Program of China (2016YFC0501604), and the Fundamental Research Funds for the Central Universities. We acknowledge the World Climate Research Programme's Working Group on Coupled Modelling, which is responsible for CMIP. We are grateful to the National Meteorological Information Center of China Meteorological Administration for archiving the observed data.

References

AghaKouchak, A., L. Cheng, O. Mazdiyasni, and A. Farahmand (2014), Global warming and changes in risk of concurrent climate extremes: Insights from the 2014 California drought, *Geophys. Res. Lett.*, *41*, 8847–8852, doi:10.1002/2014GL062308.

Fischer, E. M., S. I. Seneviratne, P. L. Vidale, D. Lüthi, and C. Schär (2007), Soil moisture–atmosphere interactions during the 2003 European summer heat wave, *J. Clim.*, *20*, 5081–5099.

Hauser, M., R. Orth, and S. I. Seneviratne (2016), Role of soil moisture versus recent climate change for the 2010 heat wave in western Russia, *Geophys. Res. Lett.*, *43*, 2819–2826, doi:10.1002/2016GL068036.

Jones, B., B. C. O'Neill, L. McDaniel, S. M. cGinnis, L. O. Mearns, and C. Tebaldi (2015), Future population exposure to US heat extremes, *Nat. Clim. Change*, *5*, 652–655.

Koenker, R., and K. Hallock (2001) Quantile regression: An introduction, *J. Econ. Perspect.*, *15*, 43–56.

Li, B., Y. Chen, Z. Chen, H. Xiong, and L. Lian (2016), Why does precipitation in northwest China show a significant increasing trend from 1960 to 2010?, *Atmos. Res.*, *167*, 275–284.

Lu, R. Y., and R. D. Chen (2016), A review of recent studies on extreme heat in China, *Atmos. Ocean. Sci. Lett.*, *9*, 114–121.

Mazdiyasni, O., and A. AghaKouchak (2015), Substantial increase in concurrent droughts and heatwaves in the United States, *Proc. Natl. Acad. Sci. U.S.A.*, *112*, 11,484–11,489.

McKee, T. B., N. J. Doesken, and J. Kleist (1993), The relationship of drought frequency and duration to time scales, in *Proceedings of the 8th Conference on Applied Climatology*, *Am. Meteorol. Soc.*, vol. 17, pp. 79–183, Boston, Mass.

Meng, L., and Y. Shen (2014), On the relationship of soil moisture and extreme temperatures in East China, *Earth Interact.*, *18*, 1–20.

Miao, C., Q. Sun, D. Kong, and Q. Duan (2016), Record-breaking heat in northwest China in July 2015: Analysis of the severity and underlying causes, *Bull. Am. Meteorol. Soc.*, *97*, S97–S101.

Miralles, D. G., A. J. Teuling, C. C. van Heerwaarden, and J. Vilà-Guerau de Arellano (2014), Mega-heatwave temperatures due to combined soil desiccation and atmospheric heat accumulation, *Nat. Geosci.*, *7*, 345–349.

Mueller, B., and A. S. I. Seneviratne (2013), Hot days induced by precipitation deficits at the global scale, *Proc. Natl. Acad. Sci. U.S.A.*, *109*, 12,398–12,403.

Otto, F. E. L., N. Massey, G. J. van Oldenborgh, R. G. Jones, and M. R. Allen (2012), Reconciling two approaches to attribution of the 2010 Russian heat wave, *Geophys. Res. Lett.*, *39*, L04702, doi:10.1029/2011GL050422.

Perkins, S. E., L. V. Alexander, and J. R. Nairn (2012), Increasing frequency, intensity and duration of observed global heatwaves and warm spells, *Geophys. Res. Lett.*, *39*, L20714, doi:10.1029/2012GL053361.

Quesada, B., R. Vautard, P. Yiou, M. Hirschi, and S. I. Seneviratne (2012), Asymmetric European summer heat predictability from wet and dry southern winters and springs, *Nat. Clim. Change*, *2*, 736–741.

Rahmstorf, S., and D. Coumou (2011), Increase of extreme events in a warming world, *Proc. Natl. Acad. Sci. U.S.A.*, *108*, 17,905–17,909.

Russo, S., A. Dosio, R. G. Graversen, J. Sillmann, H. Carrao, M. B. Dunbar, A. Singleton, P. Montagna, P. Barbola, and J. V. Vogt (2014), Magnitude of extreme heat waves in present climate and their projection in a warming world, *J. Geophys. Res. Atmos.*, *119*, 12,500–12,512, doi:10.1002/2014JD022098.

Schär, C. (2015), Climate extremes: The worst heat waves to come, *Nat. Clim. Change*, *6*, 128–129.

Seneviratne, S. I., et al. (2010), Investigating soil moisture–climate interactions in a changing climate: A review, *Earth Sci. Rev.*, *99*, 125–161.

Shen, Y., A. Xiong, Y. Wang, and P. Xie (2010), Performance of high-resolution satellite precipitation products over China, *J. Geophys. Res.*, *115*, D02114, doi:10.1029/2009JD012097.

Song, L., Y. Sun, S. Dong, B. Zhou, P. Stott, and G. Ren (2015), Role of anthropogenic forcing in 2014 hot spring in northern China, *Bull. Am. Meteorol. Soc.*, *96*, S111–S114.

Stott, P. A., D. A. Stone, and M. R. Allen (2004), Human contribution to the European heatwave of 2003, *Nature*, *432*, 610–614.

Sun, Y., et al. (2014), Rapid increase in the risk of extreme summer heat in Eastern China, *Nat. Clim. Change*, *4*, 1082–1085.

Sun, Q. H., C. Y. Miao, A. AghaKouchak, and Q. Y. Duan (2016), Century-scale causal relationships between global dry/wet conditions and the state of the Pacific and Atlantic Oceans, *Geophys. Res. Lett.*, *43*, 6528–6537, doi:10.1002/2016GL069628.

Taylor, K. E., R. J. Stouffer, and G. A. Meehl (2012), An Overview of CMIP5 and the experiment design, *Bull. Am. Meteorol. Soc.*, *93*, 485–498.

Xu, W. H., Q. X. Li, X. L. Wang, S. Yang, L. J. Cao, and Y. Feng (2013), Homogenization of Chinese daily surface air temperatures and analysis of trends in the extreme temperature indices, *J. Geophys. Res. Atmos.*, *118*, 9708–9720, doi:10.1002/jgrd.50791.

Yang, T. T., X. G. Gao, S. Sorooshian, and X. Li (2016), Simulating California reservoir operation using the classification and regression-tree algorithm combined with a shuffled cross-validation scheme, *Water Resour. Res.*, *52*, 1626–1651, doi:10.1002/2015WR017394.

Yang, T., A. Akbari Asanjan, E. Welles, X. Gao, S. Sorooshian, and X. Liu (2017), Developing reservoir monthly inflow forecasts using artificial intelligence and climate phenomenon information, *Water Resour. Res.*, *53*, doi:10.1002/2017WR020482.

You, Q., Z. Jiang, L. Kong, Z. Wu, Y. Bao, S. Kang, and N. Pepin (2016), A comparison of heat wave climatologies and trends in China based on multiple definitions, *Clim. Dyn.*, 1–15, doi:10.1007/s00382-016-3315-01-15.

Zhu, Y. L., H. J. Wang, W. Zhou, and J. H. Ma (2011), Recent changes in the summer precipitation pattern in East China and the background circulation, *Clim. Dyn.*, *36*, 1463–1473.